Accepted Manuscript

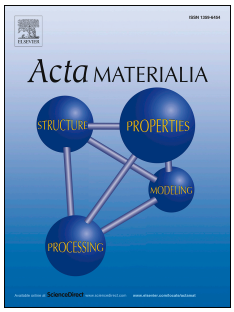

Amorphization due to electronic energy deposition in defective strontium titanate

Haizhou Xue, Eva Zarkadoula, Peng Liu, Ke Jin, Yanwen Zhang, William J. Weber

PII: S1359-6454(17)30063-0

DOI: 10.1016/j.actamat.2017.01.051

Reference: AM 13513

To appear in: *Acta Materialia*

Received Date: 19 September 2016

Revised Date: 19 January 2017

Accepted Date: 24 January 2017

Please cite this article as: H. Xue, E. Zarkadoula, P. Liu, K. Jin, Y. Zhang, W.J. Weber, Amorphization due to electronic energy deposition in defective strontium titanate, *Acta Materialia* (2017), doi: 10.1016/j.actamat.2017.01.051.

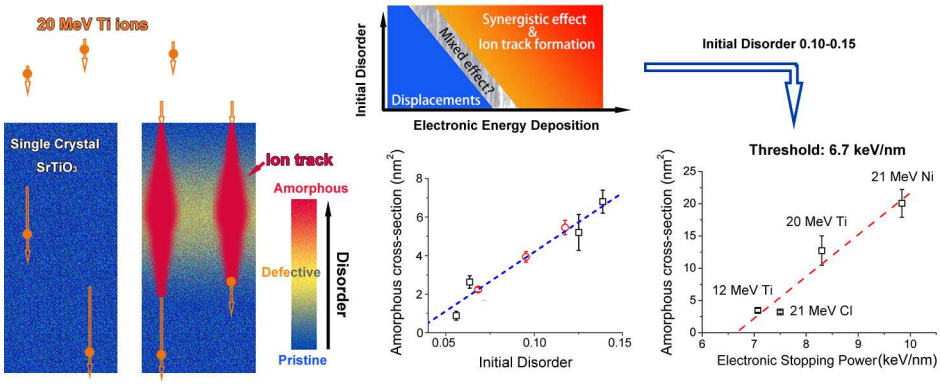

Amorphization due to electronic energy deposition in defective strontium titanate

Haizhou Xue [a], Eva Zarkadoula [b], Peng Liu [a, c], Ke Jin [c], Yanwen Zhang [b, a] and William J. Weber [a, b*]

[a] *Department of Materials Science & Engineering, University of Tennessee, Knoxville, Tennessee 37996, USA.*

[b] *Materials Science & Technology Division, Oak Ridge National Laboratory, Oak Ridge, Tennessee 37831, USA.*

[c] *School of Physics, State Key Laboratory of Crystal Materials and Key Laboratory of Particle, Physics and Particle Irradiation (MOE), Shandong University, Jinan 250100, China.*

** To whom correspondence should be addressed: wjweber@utk.edu*

Abstract

The synergistic interaction of electronic energy loss by ions with ion-induced defects created by elastic nuclear scattering processes has been investigated for single crystal $SrTiO_3$. An initial pre-damaged defect state corresponding to a relative disorder level of 0.10 to 0.15 sensitizes the $SrTiO_3$ to amorphous track formation along ion path of 12 and 20 MeV Ti, 21 MeV Cl and 21 MeV Ni, where Ti, Cl and Ni ions otherwise do not produce amorphous or damage tracks in pristine $SrTiO_3$. The electronic stopping

power threshold for ion track formation is found to be 6.7 keV/nm for the pre-damaged defect state studied in this work. These results suggest the possibility of selectively producing nanometer scale, amorphous ion tracks into thin films of epitaxial $SrTiO_3$.

Key Words: $SrTiO_3$, energy dissipation, stopping power, ion track, amorphization

1. Introduction

Ion irradiation is an important and routinely utilized tool to modify the band structure and charge density of semiconductors. On the other hand, it is also well known that ion irradiation has been proven to be a highly efficient, low cost method to simulate defect production, volume swelling and phase transformations in nuclear materials due to radioactive decay, nuclear fission, and neutron irradiation. With regard to these applications, it is important to understand and predictively model the response of electronic and nuclear materials to ion irradiation in order to develop the next generation of electro-optic-magnetic devices and more radiation tolerant nuclear materials. Therefore, a comprehensive understanding of ion-solid interactions at the level of atoms and electrons is urgently needed. Because of the complexity of ion-solid interactions, a well-accepted approaching is to separate the energy deposition from ions into (a) nuclear stopping power (S_n), which is the elastic energy loss to atomic nuclei; and (b) electronic stopping power (S_e), which is the inelastic energy loss to electrons. The understanding of S_n is relatively well established by an elastic scattering or collision model. It is known that S_n, transfers energy to target nuclei that directly results in the displacements of target atoms, which leads to the production of point defects and defect clusters. The energy loss to the electrons, its dissipation and the effects on atomic processes are, however, relatively much less understood, especially, at intermediate ion energies ranging from several hundreds of keV to tens of MeV. Recent studies have demonstrated that S_e can couple complexly

with the defects induced by S_n, which can lead to modification of the target materials in different ways [1]. For materials such as CeO_2 and ZrO_2 [2], $ZrSiO_4$ [3] and probably α-SiO_2 [4], the electronic energy loss leads to damage production that is linearly additive to the damage produced by elastic nuclear collisions. On the other hand, electronic energy loss can induce a localized thermal spike via the diffusion of free electrons and electron-phonon coupling that can cause damage recovery, such as that reported for SiC [5, 6, 7], Gd_2TiZrO_7 [1], and $(Ca,Sr)_2(La,Nd)_8(SiO_4)_6O_2$ [8]. Recently, a substantial synergistic effect has been reported for single crystal $SrTiO_3$ [5,[9, 10, 11]. Both experimental and computer simulation results confirm that the presence of a small level of pre-existing damage in single crystal $SrTiO_3$, created by nuclear collision processes, leads to the formation of amorphous ion tracks by 21 MeV Ni ions; whereas no tracks form in the pristine material. The value of S_e (9.9 keV/nm) for the 21 MeV Ni ions is below the calculated threshold of ~12 keV/nm for ion track formation in pristine $SrTiO_3$ due to track overlap [12].

In the present study, this synergistic effect in $SrTiO_3$ is further investigated in order to determine the electronic energy loss threshold for this phenomenon and the dependence on initial level of pre-damage. The motivation, on one hand, is to improve the understanding of the coupled effects of electronic and nuclear stopping power. A practical concern is that for the nuclear applications $SrTiO_3$ and similar materials are considered for the immobilization of nuclear wastes [13, 14], and a synergistic effect may dramatically accelerate damage accumulation from radioactive decay. On the

other hand, there may be beneficial applications for this synergistic effect in ion beam modification and processing, such as the selective production of nanoscale amorphous tracks (i.e., cylindrical columns) in thin film devices, with the cross-section of the amorphous track controlled by the electronic energy loss and initial defect concentration. In addition, $SrTiO_3$ is a critical foundational material in micro-electronics [15, 16, 17], and the interface it forms with other dielectric oxides and selenides, such as $LaAlO_3$ [18, 19, 20] and FeSe [21], or even with its amorphous phase [22], results in unique electronic and ferromagnetic properties of interest. By taking advantage of the synergistic effect, ion beam modification is a potential new tool for creating concentric nanometer diameter interfaces with unique functionalities for device applications.

2. Experimental

Single crystal $SrTiO_3$ samples used in this work were (100) oriented wafers obtained from the MTI Corp. The ion irradiations and Rutherford Backscattering Spectrometry in channeling geometry (RBS/C) measurements were performed using a 3 MV tandem accelerator and facilities in the Ion Beam Materials Laboratory (IBML) located at the University of Tennessee [23]. In order to produce initial pre-damaged regions with different levels of disorder in the pristine $SrTiO_3$, low energy irradiations using either 600 keV O ions at an incident angle of 60° or 900 keV Au ions at near normal incidence were performed. The RBS/C measurements revealed relatively low initial damage profiles in the $SrTiO_3$ with a peak distribution and maximum disorder

fractions ranging from 0.10 to 0.15 for 600 keV O ion irradiation to a fluence of 6.8×10^{14} cm^{-2} and 900 keV Au ion irradiation to a fluence of 3.9×10^{13} cm^{-2}. In addition, a relatively higher initial peak disorder fraction of 0.35 was produced by Au ion irradiation to a fluence of 5.4×10^{13} cm^{-2}. Both pristine samples and these pre-damaged samples were subsequently irradiated with 21 MeV Ni, 12 and 20 MeV Ti, 21 MeV Cl and 18 MeV Si ions, which have different ratios of electronic to nuclear energy loss, as summarized in Table 1. While the 600 keV O irradiation was performed at 60° relatively to the surface normal direction, all the other irradiations were performed with the incident ion beam only several degrees off the surface normal to avoid channeling effects. For the pre-damaged samples, multiple spots were irradiated with high-energy ions to fluences ranging from 10^{11} to 10^{14} cm^{-2} in order to obtain both isolated and overlapping ion paths. Before and after each ion irradiation, RBS/C measurements using 3.5 MeV He ions were performed in situ to determine the change in disorder profile of each irradiated spot with the sample remaining in place and retaining its orientation. All the ion irradiations and RBS/C measurements were carried out at room temperature in a high vacuum.

3. Thermal spike model

An inelastic thermal spike model suitable for insulators [24, 25] describes the energy exchange between the electronic and atomic subsystems due to energy deposition from a single high energy ion. The interactions can be described in terms of a set of

two heat diffusion equations, one describing the evolution of the electronic temperature T_e (Eq. 1), and the other one describing the evolution of the atomic temperature T_α (Eq. 2).

$$C_e(T_e)\frac{\partial T_e}{\partial t} = \frac{1}{r}\frac{\partial}{\partial r}\left[r\,K_e(T_e)\frac{\partial T_e}{\partial r}\right] - g(T_e - T_a) + A(r,t) \qquad (1)$$

$$C_a(T_a)\frac{\partial T_a}{\partial t} = \frac{1}{r}\frac{\partial}{\partial r}\left[r\,K_a(T_a)\frac{\partial T_a}{\partial r}\right] + g(T_e - T_a) \qquad (2)$$

Here, C_e and C_α are the heat capacities of the electronic and the atomic systems, respectively, K_e is the electronic thermal conductivity, and K_α is the thermal conductivity of the atomic system. The energy exchange between the electronic and the atomic systems depends on the temperature difference $T_e - T_a$ between them, and g, which is the electron-phonon coupling parameter, determines the strength of the interaction. The term A(r, t) describes the energy deposition from the incident ion to the electrons [26].

For the specific heat, we used C_e = 1.0 J cm^{-3} K^{-1} [24, 27] and C_α = 0.544 J cm^{-3} K^{-1} [28]. For the crystalline pristine sample, K_e is equal to $K_e = C_eD_e$ [24, 27], where D_e is the thermal diffusivity and has a value of 1.0 cm^2 s^{-1} [24, 27], K_a is 11.2 W m^{-1} K^{-1} at 300 K, and the electron-phonon coupling parameter g is 4.3×10^{18} W m^{-3} K^{-1} [24]. To account for the decreased electron mean free path due to the presence of the irradiation defects in the pre-damaged systems [29], we assumed the values of K_e and K_a are reduced by an order of magnitude relative to the values for the perfect

crystalline system, as in our previous studies [9 - 11]; likewise, we assumed that the value of g is 35% larger than the one estimated for the pristine crystalline $SrTiO_3$ [9 , 11]. The electronic energy loss for each ion was calculated using the SRIM code [30] at an irradiation depth of 100 nm.

4. Results and discussion

For the low-energy 600 keV O ions and 900 keV Au ions, their S_e values are relatively low (< 1.3 keV/nm) and far below the calculated threshold value (~12 keV/nm) for amorphous track formation in pristine $SrTiO_3$ [12]. Under these irradiation conditions, the damage production is mainly attributed to atomic displacements induced by S_n, and the kinetics are described by a direct-impact/defect-stimulated model [31]. The high energy ions, however, were chosen with S_e values that range from 6.2 to 9.9 keV/nm, as predicted by the SRIM2008 code [30] at the peak of pre-damage states. Under these high-energy irradiation conditions, the dominance of S_e over S_n produces intensive ionization that results in a highly local, radially dependent thermal spike along the ion path due to electron-phonon coupling. As shown in Table 1, the values of S_n at these high energies are negligible, and the ratios of S_e/S_n are large. Consequently, few defects are expected to be induced along the first 500 nm of ion path for the ion fluences utilized in this work. Therefore, any significant damage production must be due to the electronic energy loss. As shown in the inset of Fig. 1a, 12 and 20 MeV Ti ions do not produce significant damage in the pristine single crystal $SrTiO_3$, similar to what has been previously reported for 21 MeV Ni ions [10].

On the other hand, the RBS/C spectra in Fig. 1a clearly show damage accumulation under 20 MeV Ti irradiation when a pre-existing damage state (relative disorder peak of 0.14) is present. The backscattering yield increases rapidly and a fully amorphous state is achieved at the damage peak for an ion fluence of 1.7×10^{13} ions cm^{-2}, as evidenced by the backscattering yield reaching the random level at the channel numbers corresponding to the peak of the pre-damaged state on the Sr sublattice. Using an iterative process that is described in detail elsewhere [32], the relative disorder fraction on the Sr sublattice can be determined as a function of depth, as shown in Fig. 1b, where a relative disorder of 0 corresponds to the pristine single crystal, and 1.0 corresponds to a fully amorphous state. It is found that this rapid increase of relative disorder only occurs within the pre-damaged region, which extends to a depth of ~250 nm. In the pristine $SrTiO_3$ region beyond the pre-damage profile, little additional disorder is induced. Based on SRIM calculations, the Ti ion fluence to achieve amorphization (1.7×10^{13} ions cm^{-2}) corresponds to a displacement dose of <0.001 dpa (displacement per atom) in the pre-damaged region, which is too low to account for any measurable damage by RBS/C. Therefore, the extremely effective damage accumulation and amorphization is attributed to the intense electronic energy deposition. It is worth noting that the Ti sublattice follows the same trend as the Sr sublattice, as clearly shown in previous studies [32, 33, 34], and achieves full amorphization at the Ti damage peak for a fluence of 1.7×10^{13} ions cm^{-2}; however, due to a relatively low backscattering yield for Ti, only the Sr sublattice was analyzed to achieve better statistics. While the electronic stopping powers are lower

for 12 and 20 MeV Ti ions than for 21 MeV Ni ions (Table 1), this behavior is consistent with the production of amorphous ion tracks, as was experimentally confirmed previously for 21 MeV Ni ions in defective $SrTiO_3$ [10].

According to the two-temperature thermal spike model [25], an amorphous ion track can form in a crystalline lattice by localized thermal melting, via electron-phonon coupling, followed by an extremely rapid quench. The model suggests that energy loss to the electrons along the ion path is transferred to phonons within a few hundred femtoseconds, leading to a highly localized, radially dependent thermal spike, which may be sufficient to cause local melting and rapid quenching that creates an amorphous track along the ion path. In the thermal spike, energy deposition to electrons by the ions, electron and lattice thermal conductivities, and electron-phonon coupling of the target material play crucial roles in determining the time and radial distribution of the local temperature. In the target material, radiation-induced defects will decrease the thermal conductivity [35] and may increase the electron-phonon coupling, due to the decrease of the electron mean free path [29]. As a result, the radial energy deposition and temperature profiles become significantly localized [10, 11] with the peak temperature increasing by nearly an order of magnitude in the pre-damaged $SrTiO_3$, as illustrated in Fig. 2a. The calculated temperature profiles at 300 fs for 21 MeV Ni, 12 and 20 MeV Ti and 21 MeV Si in pre-damaged $SrTiO_3$ are shown in Fig. 2b, along with the melt temperature, T_m, for $SrTiO_3$, which provides an estimate of the maximum melt radius for each ion. Molecular dynamics (MD)

simulations of track formation in pre-damaged $SrTiO_3$ have been performed for the temperature profiles illustrated in Fig. 2b, and the results demonstrate a decrease in track diameter with decreasing values of S_e [11].

By taking advantage of a peak distribution of the initial damage profile and the depth-resolved RBS/C measurements, we are able to further study the relation between the defect concentration and the ion tracks. As discussed above, for the high energy ions, S_n induced displacements are negligible. Without effective point defect production and aggregation, the defect-stimulated growth of the amorphous domains is suppressed. Therefore, direct production and overlapping of continuous or discontinuous amorphous ion tracks due to S_e are considered to be the dominating mechanism for the observed damage accumulation. A direct impact model [36, 37] is employed as an approach in order to estimate the average amorphous cross-section (σ_a) as a function of ion fluence (Φ):

$$f_a = f_0 + (1 - f_o)\exp(-\sigma_a \bullet \Phi) \qquad (3)$$

where f_0 is the initial disorder faction induced by 900 keV Au irradiation, f_a is the disorder fraction at each ion fluence. An example is shown in Fig. 3a for initial disorder fractions of 0.06, 0.09 and 0.14 under 20 MeV Ti irradiation. The goal in this present study is to determine the electronic energy loss threshold for amorphization track formation. It has been previously demonstrated that track size increases with increasing level of existing disorder [10], so only the data for relative disorder levels of less than 0.3 are used to estimate the track cross-section. By applying the direct

impact model at different depths to the initially linear disorder accumulation, the amorphous cross-sections, as shown in Fig. 3b, exhibit a monotonically increase as a function of the initial disorder fraction. At relatively low disorder (<0.3), the RBS/C determined disorder fraction for the pre-damaged state is proportional to the concentration of irradiation-induced defects produced by the low-energy Au ions. Therefore, the results suggest that the defect profile locally changes the radial thermal spike profile, resulting in changes in the amorphous cross-section of ion tracks with depth. Moreover, a linear fitting in Fig. 3b indicates that at a low pre-damaged state, the synergistic effect is still present, which is suggested by the 20 MeV Ti irradiation results at the near surface region, where the relative disorder is initially <0.05.

Another critical factor that determines ion track formation and cross-section is the value of the electronic stopping power of the ions. The threshold electronic energy loss for amorphization due to the formation and overlap of ion tracks in pristine $SrTiO_3$ has been experimentally estimated to be 11.7 keV/nm, while calculations with the two-temperature model suggest a threshold of 12.7 keV/nm [12]. Previous results for 21 MeV Ni ions (9.9 keV/nm) demonstrated that pre-existing defects can significantly shift the threshold to much lower values of electronic energy loss. In the present study, 21 MeV Ni ions (S_e=9.9 keV/nm), 20 (S_e=8.6 keV/nm) and 12 MeV (7.1 keV/nm) Ti ions, 21 MeV Cl ions (7.1 keV/nm) and 18 MeV Si ions (6.2 keV/nm) are employed in order to vary the value of S_e and minimize S_n at the pre-damage peak. For a similar initial level of relative disorder between 0.10 and 0.15, RBS/C results

indicate that ion tracks are created in the pre-damaged regions, except for the 18 MeV Si ions, which suggests an electronic stopping power threshold above 6.2 keV/nm. The amorphous cross-sections determined from the RBS/C results are shown in Fig. 4 as a function of electronic stopping power. A linear dependence, similar to that predicted by MD simulations [11], is indicated, and a linear fit predicts a threshold in electronic stopping power of 6.7 keV/nm for amorphous ion track formation in $SrTiO_3$ pre-damaged to a disorder level of 0.10 to 0.15. The decrease in track cross section with decreasing S_e in Fig. 4 is consistent with the decrease in maximum melt radii predicted by the two temperature model in Fig. 2b; however, the measured track radii are 40 to 60% smaller than the maximum melt radii because of recrystallization processes and uncertainty in the two-temperature model parameters.

Below this threshold, the temperature along the ion path may be insufficient to cause melting of $SrTiO_3$, as a result, amorphous ion track formation is inhibited. This is confirmed by the disorder profiles derived from the RBS/C spectra for the 18 MeV Si ion irradiations (S_e=6.2 keV/nm). As shown in Fig. 5, no evidence for amorphous track formation was observed for $SrTiO_3$ pre-damaged to a local disorder level of 0.15 (grey dash line) and lower (less than 50 nm depth). However, if the relative disorder of the pre-damaged state is increased to 0.35 (green dash line), the increase in disorder level indicates that amorphous tracks are forming as a function of 18 MeV Si ion fluence. It is not surprising that with a higher initial level of pre-damage, the synergistic effect still occurs due to increased electron-phonon coupling.

According to the discussion above, the amorphous cross-section of ion tracks is proportional to the initial disorder level and S_e. Because the pre-damage profile induced by low energy ions exhibits a peak distribution, it is expected that spindle-shape ion tracks are formed and confined within to pre-damaged region. A schematic drawing of the ion tracks produced by 20 MeV Ti ions is illustrated in Fig. 6a. Moreover, such amorphous ion tracks are nanometers in diameter and dependent on the pre-damage state, as shown in Fig. 2 and Fig. 3. Therefore, it may be possible to take advantage of the synergy between S_e and S_n. Unlike swift heavy ions whose production requires a large accelerator facility, ion beam modification with intermediate energy ions can use much smaller facilities readily available in research laboratories and industry. Therefore, pre-damage with well controlled distribution profiles can be created in crystalline thin films, and nanoscale amorphous tracks of controlled diameter can be created in pre-damaged films. The spatial topographies of ion tracks may include, but are not limited to a spindle-like shape. For example, by simply using the ions and energies employed in this work, in a pre-damaged region produced by 600 keV O combined with 900 keV Au ions, a 20 MeV Ti irradiation may produce dumbbell-like ion tracks. A hypothetical representation is illustrated in Fig. 6b. The amorphous ion tracks may locally modify the electronic properties of the target materials that create the conductive paths in an insulator [38]. In addition, the ion tracks can be removed by chemical etching methods that produce the nanopore array [39, 40], which may serve as the tunnels for molecular, or the template for the growth of nanowires. Since previous studies have demonstrated that ion-beam

damage in $SrTiO_3$ can be annealed thermally [41] and by electron beams [32], it may be possible to selectively anneal the pre-damage defects, leaving behind only amorphous tracks through the films.

5. Conclusion

The synergistic interaction between electronic energy loss by high-energy ions and ion-induced defects created by elastic nuclear scattering processes has been studied for single crystal $SrTiO_3$. This work demonstrates that low initial defect concentrations, corresponding to relative disorder levels on the order of 0.10-0.15, significantly reduce the electronic energy loss threshold for amorphous track formation to ~6.7 keV/nm. Regarding to the potential applications of the synergistic effect to modify microstructure, the lengths and the amorphous cross-sections of the ion tracks can be controlled to induce amorphous channels in thin films, amorphous structures with varied topographies and to create a continuous nanometer scale concentric crystalline-amorphous interface.

Acknowledgement

This work was supported by the U.S. Department of Energy, Office of Science, Basic Energy Sciences, Materials Sciences and Engineering Division. Haizhou Xue was supported by the University of Tennessee Governor's Chair program. Peng Liu was supported by China Scholarship Council (CSC) overseas scholarship program and by

the National Natural Science Foundation of China (Grant No. 11405097) and the Natural Science Foundation of Shandong Province of China (Grant No. ZR2014AQ21).

References

[1] W. J. Weber, D. M. Duffy, L. Thomé and Y. Zhang, The role of electronic energy loss in ion beam modification of materials. Current Opinion in Solid State and Materials Science 19 (2015) 1-11.

[2] Y. Zhang, D. S. Aidhy, T. Varga, S. Moll, P. D. Edmondson, F. Namavar, K. Jin, C. N. Ostrouchov and W. J. Weber, The effect of electronic energy loss on irradiation-induced grain growth in nanocrystalline oxides. Physical Chemistry Chemical Physics 16 (2014) 8051-8059.

[3] E. Zarkadoula, M. Toulemonde and W. J. Weber, Additive effects of electronic and nuclear energy losses in irradiation-induced amorphization of zircon. Applied Physics Letters 107 (2015) 261902.

[4] M. Toulemonde, W. J. Weber, G. Li, V. Shutthanandan, P. Kluth, T. Yang, Y. Wang and Y. Zhang, Synergy of nuclear and electronic energy losses in ion-irradiation processes: The case of vitreous silicon dioxide. Physical Review B 83 (2011) 054106.

[5] Y. Zhang, T. Varga, M. Ishimaru, P. Edmondson, H. Xue, P. Liu, S. Moll, F. Namavar, C. Hardiman and S. Shannon, Competing effects of electronic and nuclear energy loss on microstructural evolution in ionic-covalent materials. Nuclear Instruments and Methods in Physics Research Section B: Beam Interactions with Materials and Atoms 327 (2014) 33-43.

[6] L. Thomé, A. Debelle, F. Garrido, P. Trocellier, Y. Serruys, G. Velisa and S. Miro, Combined effects of nuclear and electronic energy losses in solids irradiated with a dual-ion beam. Applied Physics Letters 102 (2013) 141906.

[7] Y. Zhang, R. Sachan, O. H. Pakarinen, M. F. Chisholm, P. Liu, H. Xue and W. J. Weber, Ionization-induced annealing of pre-existing defects in silicon carbide. Nature communications 6 (2015).

[8] W. J. Weber, Y. Zhang, H. Xiao and L. Wang, Dynamic recovery in silicate-apatite structures under irradiation and implications for long-term immobilization of actinides. RSC Advances 2 (2012) 595-604.

[9] E. Zarkadoula, O. H. Pakarinen, H. Xue, Y. Zhang and W. J. Weber, Predictive modeling of synergistic effects in nanoscale ion track formation. Physical Chemistry Chemical Physics 17 (2015) 22538-22542.

[10] W. J. Weber, E. Zarkadoula, O. H. Pakarinen, R. Sachan, M. F. Chisholm, P. Liu, H. Xue, K. Jin and Y. Zhang, Synergy of elastic and inelastic energy loss on ion track formation in SrTiO3. Scientific reports 5 (2015).

[11] E. Zarkadoula, H. Xue, Y. Zhang and W. J. Weber, Synergy of inelastic and elastic energy loss: Temperature effects and electronic stopping power dependence. Scripta Materialia 110 (2016) 2-5.

[12] M. Karlusić, S. Akcöltekin, O. Osmani, I. Monnet, H. Lebius, M. Jaksić and M. Schleberger, Energy threshold for the creation of nanodots on SrTiO3 by swift heavy ions. New Journal of Physics 12 (2010) 043009.

[13] K. L. Smith, G. R. Lumpkin, M. G. Blackford, M. Colella and N. J. Zaluzec, In situ radiation damage studies of LaxSr1− 3x ⁄ 2TiO3 perovskites. Journal of Applied Physics 103 (2008) 083531.

[14] W. J. Weber, A. Navrotsky, S. Stefanovsky, E. R. Vance and E. Vernaz, Materials science of high-level nuclear waste immobilization. MRS bulletin 34 (2009) 46-53.

[15] K. Szot, W. Speier, G. Bihlmayer and R. Waser, Switching the electrical resistance of individual dislocations in single-crystalline SrTiO3. Nat. Mater. 5 (2006) 312-320.

[16] J. Mannhart and D. G. Schlom, Oxide Interfaces-An Opportunity for Electronics. Science 327 (2010) 1607-1611.

[17] D. W. Reagor and V. Y. Butko, Highly conductive nanolayers on strontium titanate produced by preferential ion-beam etching. Nat. Mater. 4 (2005) 593-596.

[18] Z. Zhong, A. Tóth and K. Held, Theory of spin-orbit coupling at LaAlO3/SrTiO3 interfaces and SrTiO3 surfaces. Physical Review B 87 (2013) 161102.

[19] Z. Liu, C. Li, W. Lü, X. Huang, Z. Huang, S. Zeng, X. Qiu, L. Huang, A. Annadi and J. Chen, Origin of the two-dimensional electron gas at LaAlO3/SrTiO3 interfaces: the role of oxygen vacancies and electronic reconstruction. Physical Review X 3 (2013) 021010.

[20] G. Herranz, M. Basletić, M. Bibes, C. Carrétéro, E. Tafra, E. Jacquet, K. Bouzehouane, C. Deranlot, A. Hamzić and J.-M. Broto, High mobility in LaAlO3/SrTiO3 heterostructures: Origin, dimensionality, and perspectives. Phys. Rev. Lett. 98 (2007) 216803.

[21] S. Tan, Y. Zhang, M. Xia, Z. Ye, F. Chen, X. Xie, R. Peng, D. Xu, Q. Fan and H. Xu, Interface-induced superconductivity and strain-dependent spin density waves in FeSe/SrTiO3 thin films. Nat. Mater. 12 (2013) 634-640.

[22] Y. Chen, N. Pryds, J. E. Kleibeuker, G. Koster, J. Sun, E. Stamate, B. Shen, G. Rijnders and S. Linderoth, Metallic and insulating interfaces of amorphous SrTiO3-based oxide heterostructures. Nano letters 11 (2011) 3774-3778.

[23] Y. Zhang, M. L. Crespillo, H. Xue, K. Jin, C.-H. Chen, C. L. Fontana, J. Graham and W. J. Weber, New ion beam materials laboratory for materials modification and irradiation effects research. Nuclear Instruments and Methods in Physics Research Section B: Beam Interactions with Materials and Atoms 338 (2014) 19-30.

[24] M. Toulemonde, W. Assmann, C. Dufour, A. Meftah, F. Studer and C. Trautmann, Experimental phenomena and thermal spike model description of ion tracks in amorphisable inorganic insulators. Mat. Fys. Medd 52 (2006) 263-292.

[25] M. Toulemonde, W. Assmann, C. Dufour, A. Meftah, F. Studer and C. Trautmann, Experimental phenomena and thermal spike model description of ion tracks in amorphisable inorganic insulators. Ion Beam Science: Solved and Unsolved Problems(2006) 263-291.

[26] M. Waligorski, R. Hamm and R. Katz, The radial distribution of dose around the path of a heavy ion in liquid water. International Journal of Radiation Applications and Instrumentation. Part D. Nuclear Tracks and Radiation Measurements 11 (1986) 309-319.

[27] A. Meftah, J. Costantini, N. Khalfaoui, S. Boudjadar, J. Stoquert, F. Studer and M. Toulemonde, Experimental determination of track cross-section in Gd3Ga5O12 and comparison to the inelastic thermal spike model applied to several materials. Nuclear Instruments and Methods in Physics Research Section B: Beam Interactions with Materials and Atoms 237 (2005) 563-574.

[28] http://www.toplent.com/SrTiO3.htm (accessed September 7).

[29] W. N. Kang, B. W. Kang, Q. Y. Chen, J. Z. Wu, Y. Bai, W. K. Chu, D. K. Christen, R. Kerchner and S. I. Lee, Triple sign reversal of the Hall effect in HgBa2CaCu2O6 thin films after heavy-ion irradiation. Physical Review B 61 (2000) 722-726.

[30] J. F. Ziegler and J. P. Biersack, SRIM-2008, Stopping power and range of ions in matter. (2008).

[31]W. J. Weber, W. Jiang, S. Thevuthasan, R. E. Williford, A. Meldrum and L. A. Boatner.Defects and

Surface-Induced Effects in Advanced Perovskites, (2000) pp. 317-328: Springer.

[32] Y. Zhang, J. Lian, Z. Zhu, W. D. Bennett, L. V. Saraf, J. L. Rausch, C. A. Hendricks, R. Ewing and W. J. Weber, Response of strontium titanate to ion and electron irradiation. Journal of Nuclear Materials 389 (2009) 303-310.

[33] Y. Zhang, W. J. Weber, V. Shutthanandan and S. Thevuthasan, Non-linear damage accumulation in Au-irradiated SrTiO3. Nuclear Instruments and Methods in Physics Research Section B: Beam Interactions with Materials and Atoms 251 (2006) 127-132.

[34] Y. Zhang, J. Lian, C. M. Wang, W. Jiang, R. C. Ewing and W. J. Weber, Ion-induced damage accumulation and electron-beam-enhanced recrystallization in SrTiO3. Physical Review B 72 (2005) 094112.

[35] C. Yu, M. L. Scullin, M. Huijben, R. Ramesh and A. Majumdar, Thermal conductivity reduction in oxygen-deficient strontium titanates. Applied Physics Letters 92 (2008) 191911-191911-191913.

[36] J. F. Gibbons, Ion implantation in semiconductors—Part II: Damage production and annealing. Proceedings of the IEEE 60 (1972) 1062-1096.

[37] W. Weber, Models and mechanisms of irradiation-induced amorphization in ceramics. Nuclear Instruments and Methods in Physics Research Section B: Beam Interactions with Materials and Atoms 166 (2000) 98-106.

[38] J. H. Zollondz and A. Weidinger, Towards new applications of ion tracks. Nucl. Instrum. Methods Phys. Res. Sect. B-Beam Interact. Mater. Atoms 225 (2004) 178-183.

[39] F. Bergamini, M. Bianconi and S. Cristiani, Wet and vapor etching of tracks produced in SiO2 by Ti ion irradiation. Nucl. Instrum. Methods Phys. Res. Sect. B-Beam Interact. Mater. Atoms 257 (2007) 593-596.

[40] P. Y. Apel, I. V. Blonskaya, O. L. Orelovitch, D. Root, V. Vutsadakis and S. N. Dmitriev, Effect of nanosized surfactant molecules on the etching of ion tracks: New degrees of freedom in design of pore shape. Nuclear Instruments and Methods in Physics Research Section B: Beam Interactions with Materials and Atoms 209 (2003) 329-334.

[41] J. Rankin, J. McCallum and L. Boatner, The effect of annealing environments on the epitaxial recrystallization of ion-beam-amorphized SrTiO3. Journal of materials research 7 (1992) 717-724.

Table 1. Stopping powers and ratio for ions with varied energy at 100 nm in depth.

Ion	Energy (MeV)	Incident angle (°)*	S_e (keV/nm)	S_n (keV/nm)	S_e/S_n	Ion range (μm)
Ni	21	7	9.9**	0.084**	118	3.9
Ti	12	7	7.1	0.080	89	2.9
	20	7	8.6	0.050	172	3.9
Cl	21	7	7.5	0.019	394	4.2
Si	18	7	6.2	0.013	477	4.1
O	0.6	60	1.3**	0.22**	15	0.34
Au	0.9	7	0.86	4.5	0.19	0.13

* Incident angle refers to the angle between ion beam and the surface normal of $SrTiO_3$ wafer.

** For 21 MeV Ni ion irradiation, the initial damage was induced by 600 keV O ions at an I-angle of 60°; all the other irradiations were performed on the pre-damage states which are produced by 900 keV Au ions. Therefore, only for the combination of 21 MeV Ni and 600 keV O, S_e and S_n are the values at 180 nm (depth of the pre-damage peak).

Figure 1

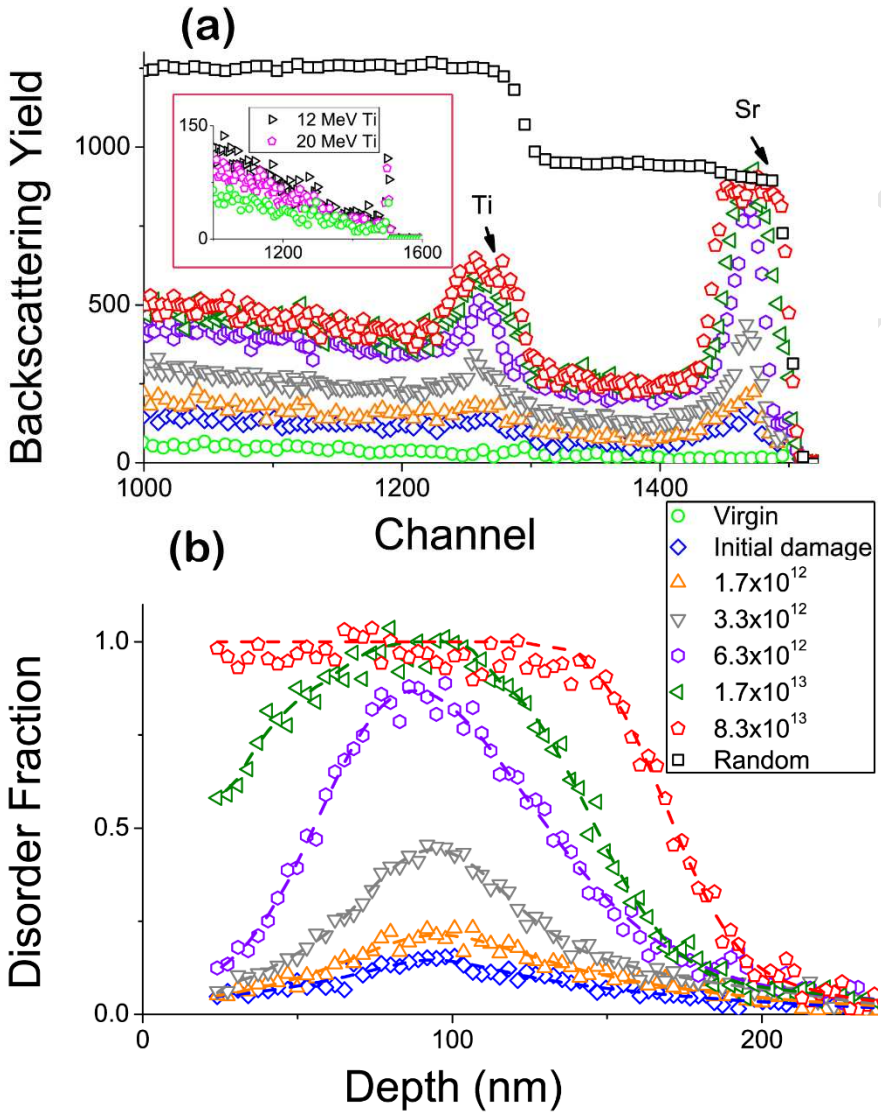

Fig. 1. (a) The RBS spectra of 20 MeV Ti irradiated single crystal $SrTiO_3$ with an initial damage created by 900 keV Au ions. The inset is the RBS/C result for 12 and 20 MeV Ti irradiations on pristine $SrTiO_3$, with identical ion fluence of 8.3×10^{13} cm^{-2}. (b) The disorder fraction profiles determined from the RBS/C spectra. The Au irradiation-induced relative disorder at the damage peak is 0.14, indicated as "initial damage".

Figure 2

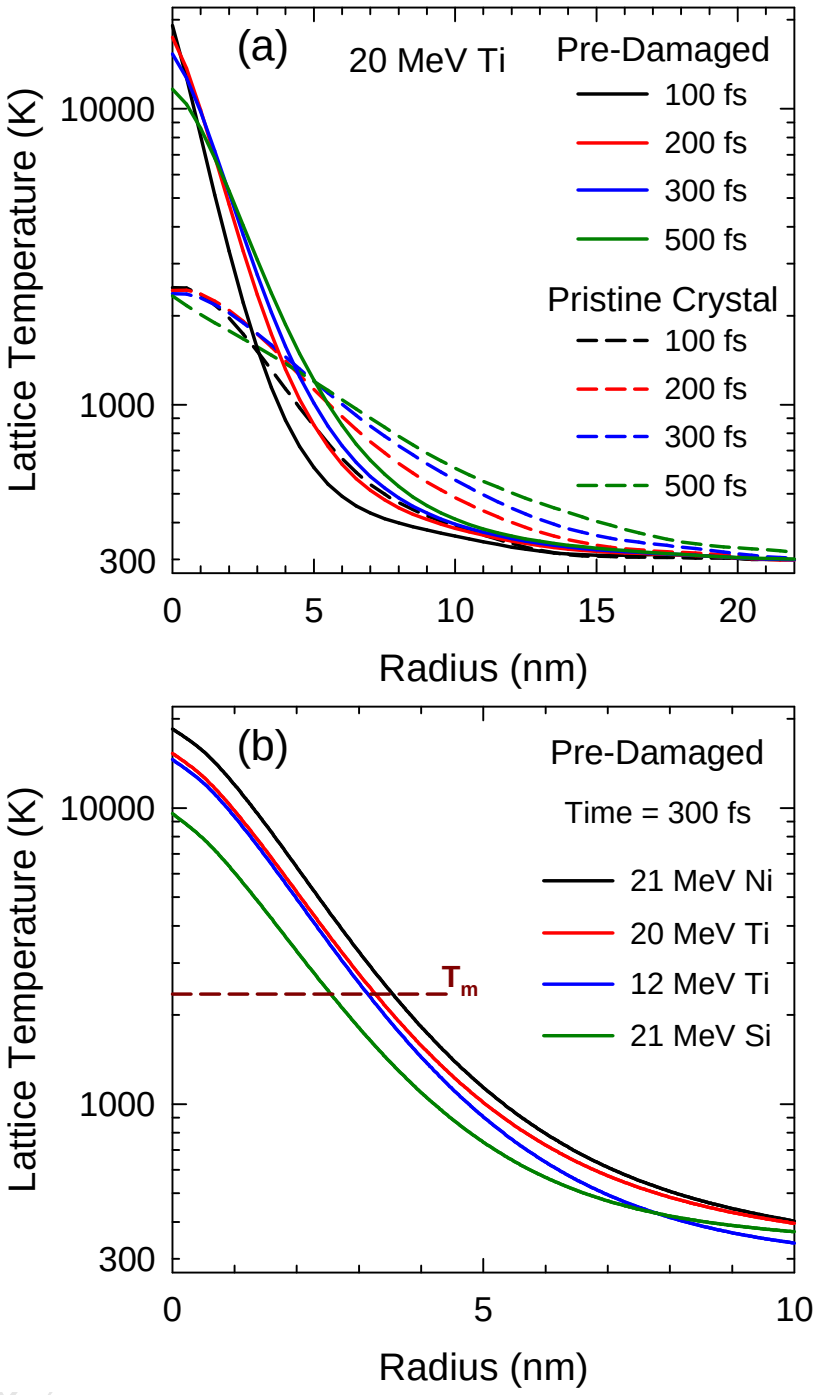

Fig 2. (a) Radial temperature profile as the function of time for 20 MeV Ti ions in pristine and pre-damaged $SrTiO_3$, and (b) Maximum temperature profiles (at 300 fs) for several ions in pre-damaged $SrTiO_3$. The melting temperature, T_m, for $SrTiO_3$ is included for reference.

Figure 3

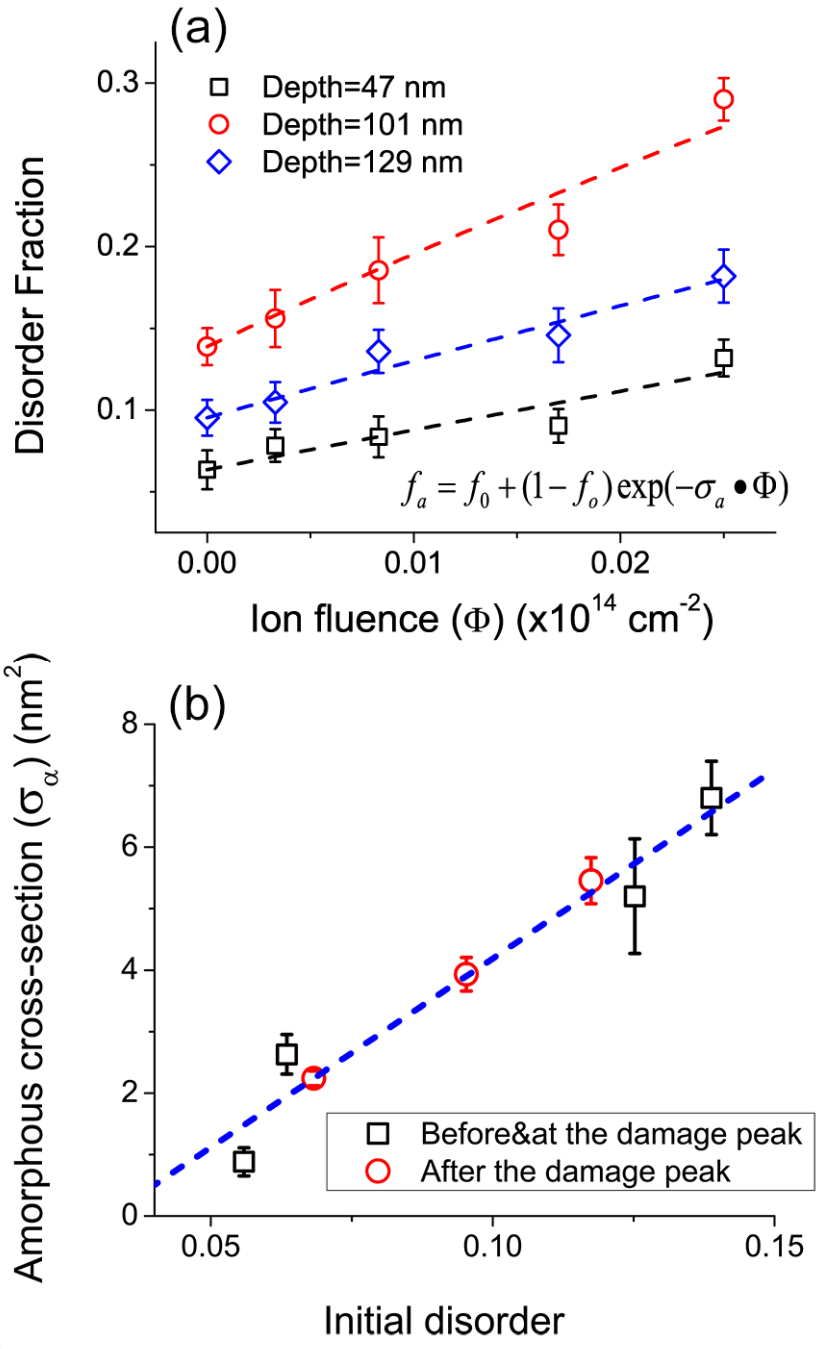

Fig. 3. (a) An example of amorphous cross-section (σ_α) estimation according to the direct-impact model (Eq. 3), for the 20 MeV Ti irradiated $SrTiO_3$ at different depths from the surface. (b) The amorphous cross-section as the function of initial disorder, before and after the damage peak (locates at ~100 nm). Standard deviations from RBS/C measurements and direct-impact model fitting are presented in the form of error bars.

Figure 4

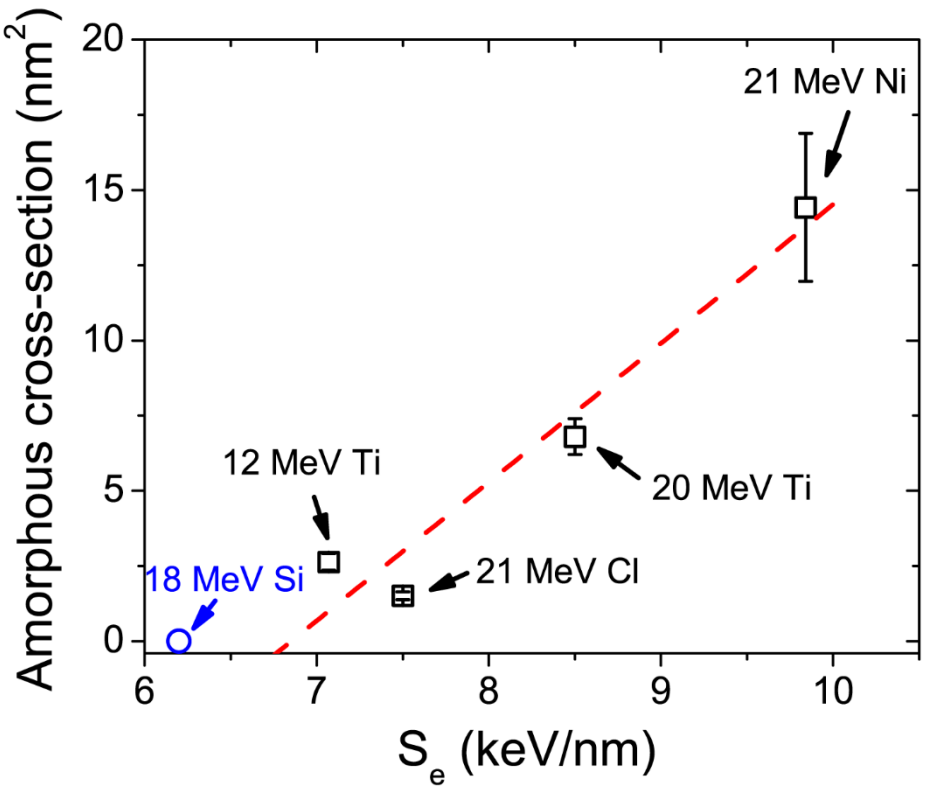

Fig. 4. The amorphous cross-sections of the ion tracks as the function of S_e, for 21 MeV Ni, 12 and 20 MeV Ti, and 21 MeV Cl ion irradiations on $SrTiO_3$ with an initial disorder fraction between 0.10 and 0.15. A linear fitting is applied, which suggests a threshold value of 6.7 keV/nm. Below this threshold and for an identical pre-damage condition, 18 MeV Si ions do produce tracks in defective $SrTiO_3$.

Figure 5

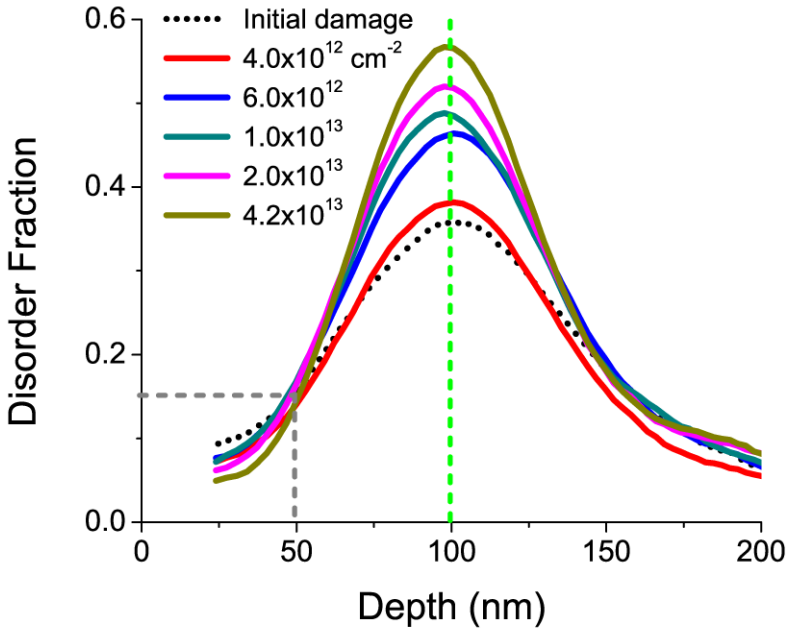

Fig. 5. Evolution of relative disorder fraction (derived from the RBS/C spectra) as the function of ion fluence for 18 MeV Si irradiation. No significant synergistic effect is found for initial disorder <0.15 after the Si irradiation; meanwhile amorphous ion tracks are produced and accelerate the damage accumulation for initial disorder ~0.35.

Figure 6

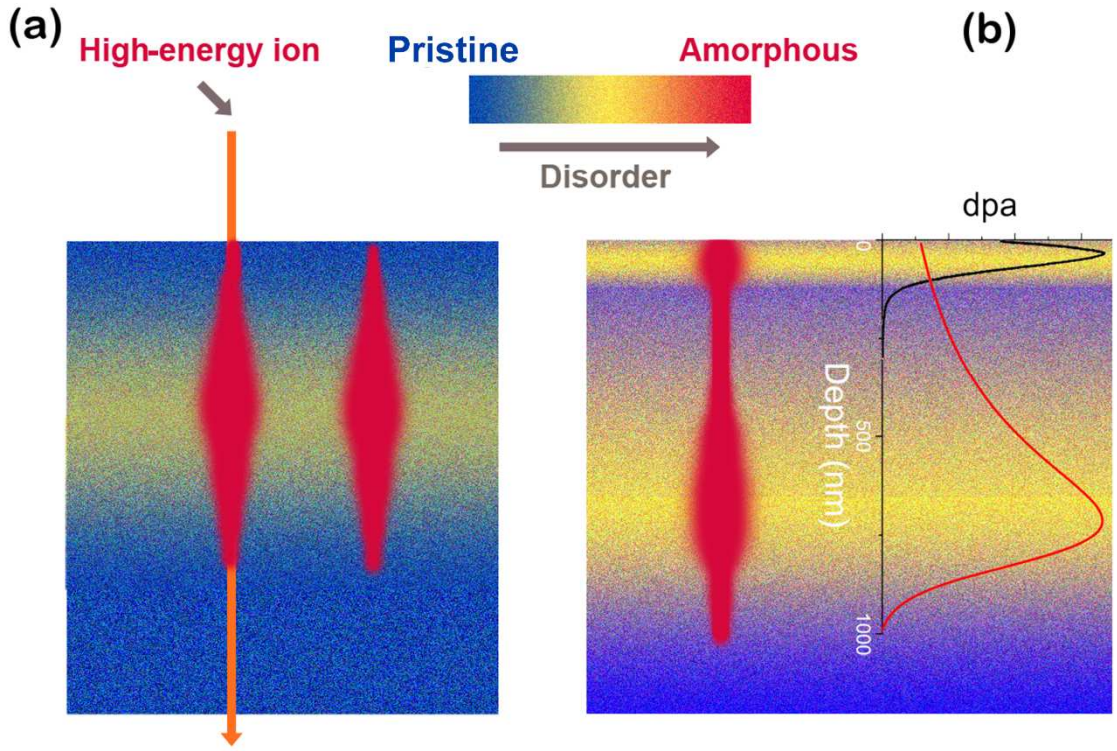

Fig. 6. (a) Schematic drawing of the spindle-like amorphous ion tracks, which are produced by 20 MeV Ti irradiation in the pre-damaged $SrTiO_3$. (b) A hypothetical representation for the initial disorder profile produced by a 900 keV Au irradiation (black curve), 60° off the surface normal direction together with a 600 keV O irradiation (red curve), 7° off the surface normal direction. Then a 20 MeV Ti irradiation is applied to create the dumbbell-shape ion tracks.